Radiative charge transfer between H and C^{++}, C^{+++}, and N^{++}

S. E. Butler, S. L. Guberman, and A. Dalgarno
Center for Astrophysics, Harvard College Observatory and Smithsonian Astrophysical Observatory, Cambridge, Massachusetts 02138
(Received 28 February 1977)

Ab initio calculations of radiative charge-transfer rate coefficients are described for C^{++}, C^{+++}, and N^{++} ions in collision with atomic hydrogen at temperatures up to 10^5 K. The rate coefficients increase slowly with increasing temperature and attain values between 2×10^{-14} and 6×10^{-14} cm^3sec^{-1} at 10^4 K.

I. INTRODUCTION

Charge-transfer processes between multiply charged ions and neutral atoms exert a significant influence on the ionization structure of laboratory and astrophysical plasmas. If favorable crossings occur of the potential curves of the initial and final diabatic states, processes such as

$$X^{m+}+A\rightarrow X^{(m-n)+}+A^{n+} \tag{1}$$

can be rapid at thermal energies.[1] In the absence of favorable crossings, charge transfer will often be more efficient when it occurs with the emission of a photon;

$$X^{m+}+A\rightarrow X^{(m-n)+}+A^{n+}+h\nu\,. \tag{2}$$

We report in this paper the rate coefficients of the radiative charge-transfer processes:

$$C^{2+}+H\rightarrow C^{+}+H^{+}+h\nu\,, \tag{3}$$

$$C^{3+}+H\rightarrow C^{2+}+H^{+}+h\nu\,, \tag{4}$$

$$N^{2+}+H\rightarrow N^{+}+H^{+}+h\nu\,. \tag{5}$$

We used the Born-Oppenheimer approximation for the calculation of the potential-energy curves and transition-dipole moments of the molecular states temporarily formed during the collision. In Tables I, II, and III, we list the initial and final channels, their associated internal energies, and the molecular states that can be formed by the separated atomic systems. In our charge-transfer calculations, we considered only those states that separate into valence states of the ions and that can couple by an allowed electric dipole transition to the initial states.

TABLE I. Channel energies for $C^{++}+H\rightarrow C^{+}+H^{+}+\Delta E$.

Separated atoms	Molecular state	ΔE (eV) Calc.	Expt.
$C^{+}(2s^22p,{}^2P^o)+H^{+}$	$1\,^2\Sigma^+$	9.86	10.78
$C^{+}(2s^22p,{}^2P^o)+H^{+}$	$1\,^2\Pi$	9.81	10.78
$C^{++}(2s^2,{}^1S)+H$	$2\,^2\Sigma^+$	0	0

II. WAVE FUNCTIONS

The electronic wave functions χ_n were expressed in terms of products of spherical harmonics and normalized Gaussian-type radial functions centered on each nucleus. The primitive basis[2] set consisted of nine s-type and five p-type Gaussian functions $(9s/5p)$ centered on the heavy nucleus, and four s-type and three p-type Gaussian functions $(4s/3p)$ centered on the hydrogen nucleus. The functions were contracted into $[3s/2p]$ and $[2s/2p]$ sets, respectively, using contraction rules developed by Dunning.[3] No π functions were included in the set centered on the hydrogen nucleus. The contracted basis sets contain 13 functions and have sufficient flexibility to describe molecular distortion and polarization effects. The contraction coefficients were averaged in order to achieve comparable accuracies in the calculation of the energies of the excited ionic states.

Hartree-Fock wave functions, which correctly describe the dissociation in the exit channels of each N-electron molecular spin multiplet, were calculated for the ground state of each multiplet at six internuclear distances R between $2a_0$ and

TABLE II. Channel energies for $C^{+++}+H\rightarrow C^{++}+H^{+}+\Delta E$.

Separated atoms	Molecular state	ΔE (eV) Calc.	Expt.
$C^{++}(2s^2,{}^1S)+H^{+}$	$1\,^1\Sigma^+$	34.2	34.3
$C^{++}(2s2p,{}^3P^o)+H^{+}$	$1\,^3\Sigma^+$	27.4	27.8
	$1\,^3\Pi$	27.3	27.8
$C^{++}(2s2p,{}^1P^o)+H^{+}$	$2\,^1\Sigma^+$	20.0	21.6
	$1\,^1\Pi$	19.8	21.6
$C^{++}(2p^2,{}^3P)+H^{+}$	$2\,^3\Pi$	16.5	17.2
$C^{++}(2p^2,{}^1D)+H^{+}$	$2\,^1\Pi$	14.5	16.2
	$3\,^1\Sigma^+$	14.6	16.2
$C^{++}(2p^2,{}^1S)+H^{+}$	$4\,^1\Sigma^+$	10.0	11.7
$C^{+++}(1s^22s,{}^2S)+H$	$5\,^1\Sigma^+$	0	0
	$2\,^3\Sigma^+$	0	0

TABLE III. Channel energies for $N^{++}+H \rightarrow N^{+}+H^{+}+\Delta E$.

Separated atoms	Molecular state	ΔE (eV) Calc.	Expt.
$N^{+}(2s^2 2p^2, {}^3P)+H^{+}$	$1\,{}^3\Pi$	15.2	16.0
	$1\,{}^3\Sigma^-$	15.1	16.0
$N^{+}(2s^2 2p^2, {}^1D)+H^{+}$	$1\,{}^1\Pi$	13.0	14.1
	$1\,{}^1\Delta$	12.9	14.1
	$1\,{}^1\Sigma^+$	12.8	14.1
$N^{+}(2s^2 2p^2, {}^1S)+H^{+}$	$2\,{}^1\Sigma^+$	10.7	11.9
$N^{+}(2s2p^3, {}^3D^o)+H^{+}$	$1\,{}^3\Pi$	3.4	4.6
	$1\,{}^3\Delta$	3.4	4.6
	$2\,{}^3\Sigma^-$	3.3	4.6
$N^{++}(2s^2 2p, {}^2P^o)+H$	$1\,{}^3\Sigma^+$	0	0
	$3\,{}^3\Pi$	0	0
	$2\,{}^1\Pi$	0	0
	$3\,{}^1\Sigma^+$	0	0

$10a_0$. Virtual orbitals appropriate to motion in the field of the $N-1$ electrons occupying the frozen orbital Hartree-Fock ground-state system were then obtained at each R by the variational method and the sets of thirteen ground-state and virtual orbitals were used to construct configuration-interaction wave functions for the excited molecular states of each multiplet. As long as the core does not undergo substantial orbital adjustment upon excitation, these improved virtual orbitals[4] provide a reliable description of the excited electrons and permit a ready physical interpretation of the configuration-interaction wave functions. At large separations one of the orbitals tends to a 1s orbital attached to the hydrogen nucleus, permitting the ready identification of the entrance channel in the scattering process.

Configuration-interaction calculations were performed for each molecular symmetry at each internuclear distance. In all cases the core 1σ orbitals on the heavy ion were unexcited and remained doubly occupied. For reactions (3) and (4) a full configuration-interaction calculation was performed for the remaining electrons, but for reaction (5) quadruple and higher excitations were omitted. Table IV lists the number of spatial configurations and spin eigenfunctions used for each molecular symmetry. Tests of the effects on the energy of the omission of the quadruple excitations in NH^{++} showed them to be negligible.

The computer programs used were developed from earlier programs constructed at the California Institute of Technology.

TABLE IV. Numbers of spatial configurations and spin eigenfunctions.

System	Molecular state	Number of spatial configurations	Number of spin eigenfunctions
CH^{++}	$^2\Sigma^+$	160	232
	$^2\Pi$	80	138
CH^{+++}	$^1\Sigma^+$	42	42
	$^3\Pi$	16	16
	$^1\Pi$	16	16
	$^3\Sigma^+$	30	30
NH^{++}	$^3\Pi$	220	424
	$^1\Pi$	220	322
	$^1\Sigma^+$	266	347
	$^3\Sigma^+$	311	519
	$^3\Sigma^-$	84	228

III. RESULTS

Figures 1, 2, and 3 show the computed potential curves for CH^{++}, CH^{+++}, and NH^{++}. The pertinent

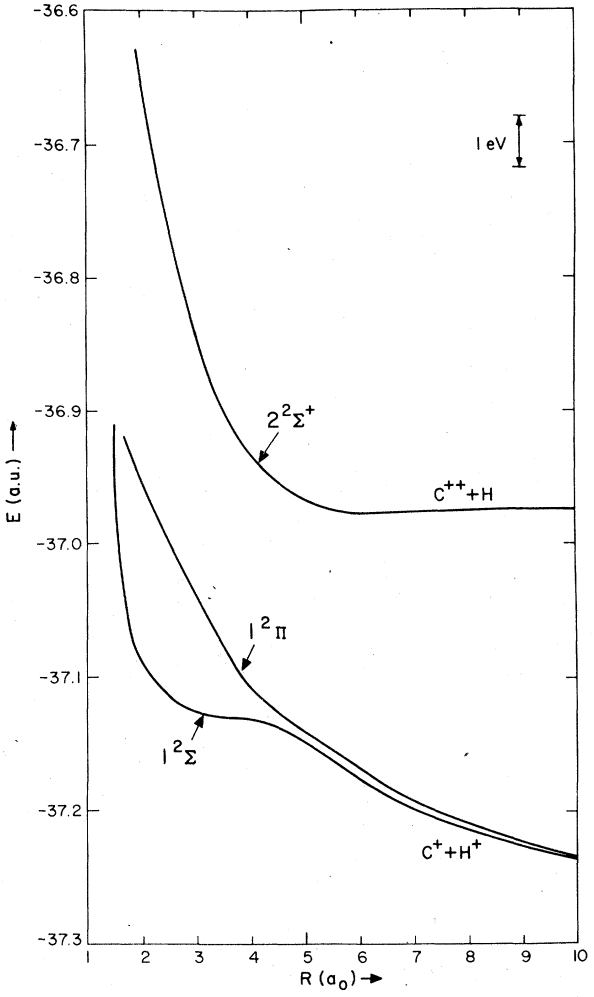

FIG. 1. Interaction potentials of CH^{++}. The incoming channel is $2^2\Sigma^+$.

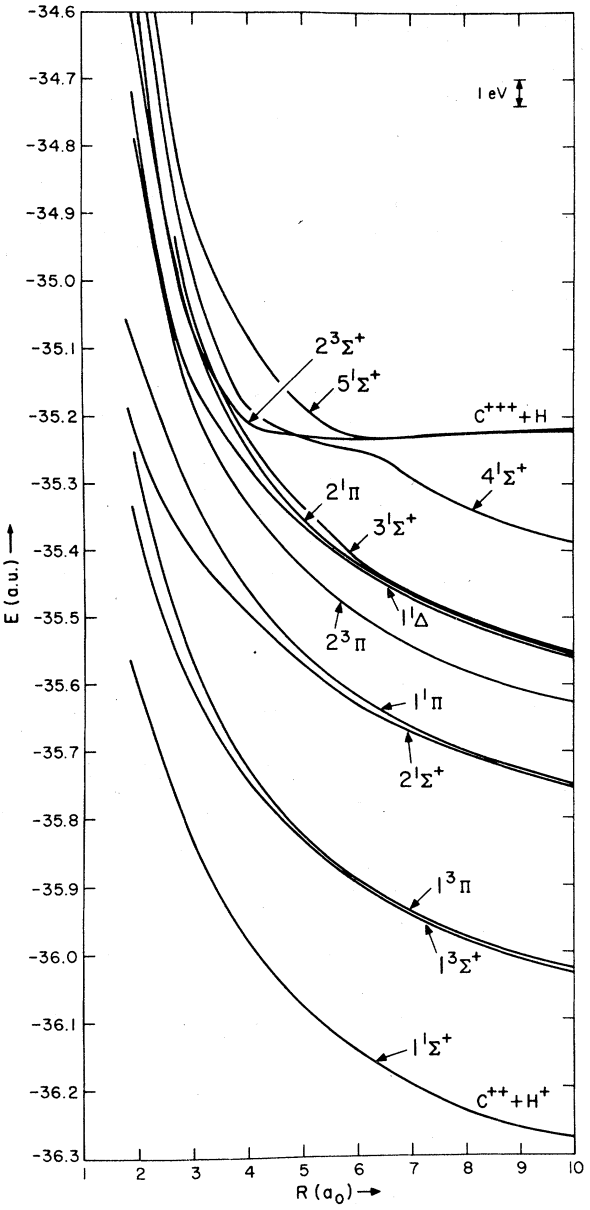

FIG. 2. Interaction potentials of CH^{+++}. The incoming channels are $2\,^3\Sigma^+$ and $5\,^1\Sigma^+$. There is an avoided crossing of $5\,^1\Sigma^+$ with $4\,^1\Sigma^+$ at $R \approx 6a_0$.

roots are numbered in order of increasing energy at $R = 10.0\ a_0$. At large separations the potential-energy curves are controlled by the R^{-1} Coulomb repulsion in the exit channels and the R^{-4} polarization attraction in the entrance channel. At smaller separations there occur several avoided crossings which are particularly evident in Figs. 2 and 3.

Tables I, II, and III list the differences between the experimental energies of the entrance and exit channels and between the configuration-interaction energies of the entrance and exit channels. The calculated differences were obtained from the configuration-interaction energies at $R = 10.0a_0$ by applying the formula

$$\Delta E(\infty) = \Delta E(R = 10a_0) + (Z - 1)/R + \tfrac{1}{2}\,\alpha(Z^2/R^4)\,,$$

where $\Delta E(\infty)$ is the asymptotic energy difference, Z is the excess charge of the incident ion, α is the polarizability of the hydrogen atom, and all quantities are expressed in atomic units. Because of the smaller correlation energy in the entrance channel in which at large separations one electron is localized near the hydrogen nucleus, the configuration-interaction calculations predict the energy of the entrance channel more accurately than the energies of the exit channels. The predicted excitation energies are accordingly smaller than

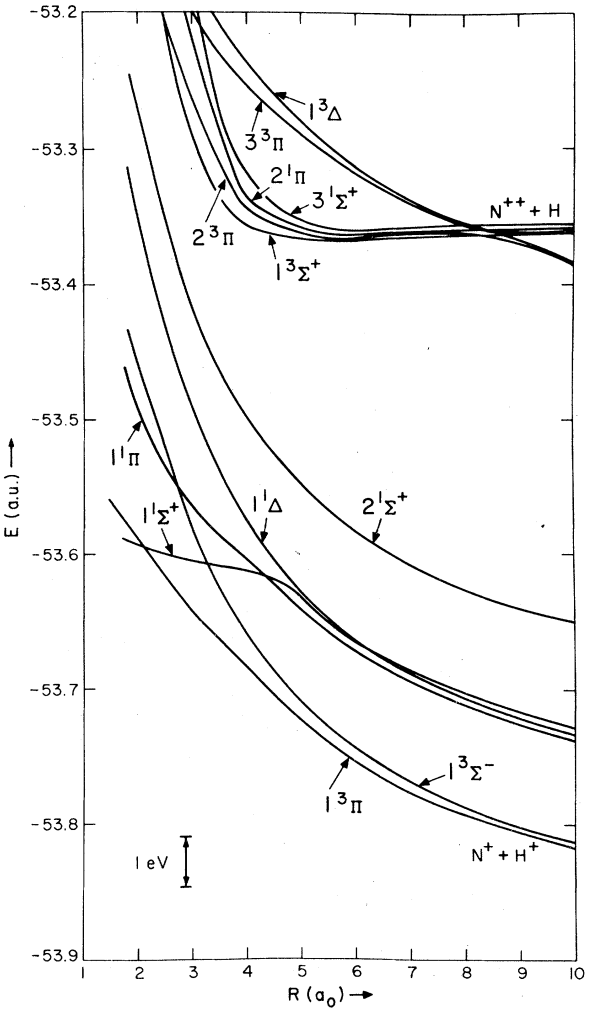

FIG. 3. Interaction potentials of NH^{++}. The incoming channels are $3\,^3\Pi$, $2\,^1\Pi$, $3\,^1\Sigma^+$, and $1\,^3\Sigma^+$. There is an avoided crossing of $3\,^3\Pi$ with $2\,^3\Pi$ at $R \approx 8a_0$.

TABLE V A. Dipole moments for transitions in CH^{++} in a.u.

R (a_0)	$2\,^2\Sigma^+$-$1\,^2\Sigma^+$	$2\,^2\Sigma^+$-$1\,^2\Pi$
10	0.0134	0.0016
8	0.0850	0.0101
6	0.4242	0.0349
4	1.1419	0.0332
3	0.2177	0.0553
2	−0.4713	0.0620

TABLE V B. Dipole moments for transitions in CH^{+++} in a.u.

R (a_0)	$5,4\,^1\Sigma^+$-$1\,^1\Sigma^+$	$5,4\,^1\Sigma^+$-$2\,^1\Sigma^+$	$5,4\,^1\Sigma^+$-$3\,^1\Sigma^+$	$5,4\,^1\Sigma^+$-$1\,^1\Pi$
10	0.0076	−0.0042	0.0031	−0.0009
8	0.0255	−0.0286	0.0212	−0.0057
6	0.0597	0.0864	0.0980	−0.0323
4	0.0680	−1.0167	1.3335	−0.0426
3	0.1254	−1.1569	1.3649	0.1024
2	−0.1693	0.6811	0.7046	−0.3096
R (a_0)	$5,4\,^1\Sigma^+$-$2\,^1\Pi$	$2\,^3\Sigma^+$-$1\,^3\Sigma^+$	$2\,^3\Sigma^+$-$1\,^3\Pi$	$2\,^3\Sigma^+$-$2\,^3\Pi$
10	0.0024	−0.0050	0.0031	0.0005
8	0.0023	−0.0343	0.0139	0.0019
6	−0.2580	−0.1407	0.0283	0.0045
4	0.1481	−0.4681	0.0145	0.0110
3	0.1516	−0.7477	−0.0344	0.0198
2	−0.8548	−0.6135	−0.0972	0.0295

TABLE V C. Dipole moments for transitions in NH^{++} in a.u.

R	$2\,^1\Pi$-$1\,^1\Sigma^+$	$2\,^1\Pi$-$1\,^1\Delta$	$2\,^1\Pi$-$2\,^1\Sigma^+$	$2\,^1\Pi$-$1\,^1\Pi$	$3\,^1\Sigma^+$-$1\,^1\Sigma^+$
10	0.0002	−0.0005	−0.0003	−0.0006	−0.0081
8	0.0014	−0.0050	−0.0028	−0.0426	−0.0574
6	0.0051	−0.0241	−0.0132	−0.2283	−0.3082
4	−0.0034	−0.0540	−0.0200	−0.8270	−1.0881
3	−0.0669	−0.0549	0.0134	−0.9768	−1.2910
2	−0.7012	−0.0521	0.1674	0.2168	−0.9455
R	$3\,^1\Sigma^+$-$2\,^1\Sigma^+$	$3\,^1\Sigma^+$-$1\,^1\Pi$	$3,2\,^3\Pi$-$1\,^3\Pi$	$3,2\,^3\Pi$-$3\Sigma^-$	$1\,^3\Sigma^+$-$1\,^3\Pi$
10	−0.0042	−0.0005	−0.0051	−0.0009	−0.0013
8	−0.0287	−0.0050	−0.0134	−0.0268	−0.0099
6	−0.1448	−0.0249	−0.1639	−0.0445	−0.0412
4	−0.3963	−0.0682	−0.5748	−0.0910	−0.0927
3	−0.2616	−0.1092	−0.1406	−0.0991	−0.1196
2	0.1109	−0.2774	−0.5141	+0.0424	−0.3624

the experimental values.

The dipole matrix element for a parallel transition between electronic states $\chi_n(\vec{\mathbf{r}}\,|R)$ and $\chi_{n'}(\vec{\mathbf{r}}|R)$, where $\vec{\mathbf{r}}$ denotes collectively the position vectors $\vec{\mathbf{r}}_i$ of all the electrons, is given in atomic units by

$$D_{nn'}(R)=\int \chi_n^*(\vec{\mathbf{r}}\,|R)\left(\sum_i z_i\right)\chi_{n'}(\vec{\mathbf{r}}\,|R)\,dR\,,$$

where $\vec{\mathbf{r}}_i=(x_i,y_i,z_i)$ and the z axis is taken along the internuclear axis. For a perpendicular transition

$$D_{nn'}(R)=\int \chi_n^*(\vec{\mathbf{r}}\,|R)\sum_i \frac{i}{\sqrt{2}}\,(x_i+iy_i)\chi_{n'}(\vec{\mathbf{r}},R)\,dR\,.$$

Using the configuration-interaction wave func-

TABLE VI. Hartree-Fock (HF) and configuration interaction (CI) dipole moments.

	NH^{++} $2\,^1\Pi$-$1\,^1\Pi$		NH^{++} $3\,^1\Sigma^+$-$1\,^1\Pi$		CH^{+++} $2\,^3\Sigma^+$-$1\,^3\Pi$		CH^{+++} $2\,^3\Sigma^+$-$1\,^3\Sigma^+$	
R	HF	CI	HF	CI	HF	CI	HF	CI
3	−0.9546	−0.9768	−0.0076	−0.1092	0.0098	−0.0344	−1.2691	−0.7477
4	−0.6806	−0.8270	−0.0148	−0.0682	0.0369	0.0145	−1.3281	−0.4681
6	−0.1645	−0.2283	−0.0080	−0.0249	0.0248	0.0283	−0.4363	−0.1407
8	−0.0288	−0.0426	−0.0017	−0.0050	0.0074	0.0139	−0.0858	−0.0343
10	−0.0039	−0.0006	−0.0002	−0.0005	0.0017	0.0031	−0.0135	−0.0050

tions, the dipole moment matrix elements were calculated for the allowed transitions for reactions (3), (4), and (5) at each internuclear distance. The results are presented in Tables V A, V B, and V C. Avoided crossings occur in the $3^3\Pi$ curve of $N^{++}-H$ and the $5^1\Sigma^+$ curve of $C^{+++}-H$. In calculating the dipole moments we assumed that the crossings occur, and that the dipole moments listed for

TABLE VII A. Rate coefficients k for charge transfer $C^{++}+H \rightarrow C^{+}+H^{+}+h\nu$.

Transition T (K)	$2\,^2\Sigma^+$-$1\,^2\Sigma^+$ k (10^{-14} cm^3 sec^{-1})	$2\,^2\Sigma^+$-$1\,^2\Pi$ k (10^{-17} cm^3 sec^{-1})
10	1.58	6.35
30	1.54	6.48
100	1.49	6.87
300	1.39	7.32
1 000	1.27	6.88
3 000	1.34	6.14
10 000	1.71	5.84
30 000	2.12	6.16
100 000	2.44	7.21

TABLE VII B. Rate coefficients k for charge transfer $C^{+++}+H \rightarrow C^{++}+H^{+}+h\nu$.

Transition T (K)	$2\,^3\Sigma^+$-$1\,^3\Sigma^+$ k (10^{-14} cm^3 sec^{-1})	$2\,^3\Sigma^+$-$1\,^3\Pi$ k (10^{-15} cm^3 sec^{-1})	$2\,^3\Sigma^+$-$2\,^3\Pi$ k (10^{-18} cm^{-3} sec^{-1})	$5,4\,^1\Sigma^+$-$2\,^1\Pi$ k (10^{-16} cm^3 sec^{-1})
10	4.90	1.09	2.36	9.26
30	4.76	1.10	2.38	9.40
100	4.57	1.14	2.43	9.84
300	4.37	1.19	2.51	10.8
1 000	4.05	1.22	2.53	11.6
3 000	3.87	1.17	2.44	10.7
10 000	4.01	1.10	2.35	9.75
30 000	4.55	1.04	2.28	9.00
100 000	5.73	1.05	2.41	8.77

Transition T (K)	$5,4\,^1\Sigma^+$-$1\,^1\Pi$ k (10^{-16} cm^3 sec^{-1})	$5,4\,^1\Sigma^+$-$1\,^1\Sigma^+$ k (10^{-15} cm^3 sec^{-1})	$5,4\,^1\Sigma^+$-$2\,^1\Sigma^+$ k (10^{-15} cm^3 sec^{-1})	$5,4\,^1\Sigma^+$-$3\,^1\Sigma^+$ k (10^{-15} cm^3 sec^{-1})
10	3.03	3.62	8.32	1.58
30	3.04	3.69	8.09	1.57
100	3.09	3.86	7.80	1.57
300	3.18	4.20	7.49	1.58
1 000	3.05	4.40	6.93	1.50
3 000	2.58	4.05	6.54	1.30
10 000	2.32	3.78	7.74	1.24
30 000	2.17	3.76	11.2	1.26
100 000	2.79	4.06	17.1	1.40

TABLE VII C. Rate coefficients k for charge transfer $N^{++} + H \rightarrow N^{+} + H^{+} + h\nu$.

Transition	$3,2\,^3\Pi$-$1\,^3\Pi$	$1\,^3\Sigma^+$-$1\,^3\Pi$	$2\,^1\Pi$-$1\,^1\Sigma^+$	$2\,^1\Pi$-$1\,^1\Delta$	$2\,^1\Pi$-$2\,^1\Sigma^+$
T (K)	k (10^{-14} cm^3 sec^{-1})	k (10^{-16} cm^3 sec^{-1})	k (10^{-18} cm^3 sec^{-1})	k (10^{-17} cm^3 sec^{-1})	k (10^{-18} cm^3 sec^{-1})
10	1.71	3.42	4.45	2.50	2.70
30	1.70	3.34	4.45	2.50	2.73
100	1.70	3.16	4.54	2.57	2.85
300	1.63	2.95	4.48	2.55	2.89
1 000	1.51	2.74	4.19	2.40	2.76
3 000	1.45	2.46	3.83	2.28	2.58
10 000	1.43	2.41	3.81	2.31	2.47
30 000	1.49	2.79	40.1	2.50	2.78
100 000	1.54	5.06	654	2.92	8.98
Transition	$2\,^1\Pi$-$1\,^1\Pi$	$3\,^1\Sigma^+$-$1\,^1\Sigma^+$	$3\,^1\Sigma^+$-$2\,^1\Sigma^+$	$3\,^1\Sigma^+$-$1\,^1\Pi$	$3,2\,^3\Pi$-$1\,^3\Sigma^-$
T (K)	k (10^{-15} cm^3 sec^{-1})	k (10^{-15} cm^3 sec^{-1})	k (10^{-16} cm^3 sec^{-1})	k (10^{-17} cm^3 sec^{-1})	k (10^{-16} cm^3 sec^{-1})
10	3.02	2.64	2.29	1.46	5.65
30	2.98	2.62	2.29	1.46	5.73
100	2.99	2.65	2.35	1.51	6.00
300	2.90	2.48	2.22	1.43	6.15
1 000	2.72	2.15	1.91	1.23	5.69
3 000	2.72	2.16	1.82	1.18	5.40
10 000	3.26	2.83	2.05	1.39	5.50
30 000	4.45	4.57	2.44	2.22	5.77
100 000	5.59	8.23	2.84	7.27	6.02

transitions originating in the $3^3\Pi$ and $5^1\Sigma^+$ states correspond to the diabatic states. As the internuclear distance decreases, the dipole moments increase exponentially. The initial behavior reflects the increase of the overlap of the product of the transition moment operator and the compact $1s$ orbital of the hydrogen atom with the $2p$ orbital of the ion. The dipole matrix element is approximately proportional to the amplitude of the $2p$ orbital at the hydrogen nucleus. Because of the smaller overlap of the product of the π orbitals and the perpendicular transition operator with the orbital associated with the hydrogen atom, the dipole moments of transitions in which $\Delta\lambda = 0$ are usually larger than those of transitions in which λ changes. Cancellation effects arising from the large number of contributing configurations produce a complicated pattern at smaller internuclear distances, and changes of sign are not uncommon.

The errors of the improved virtual orbital approximation for the prediction of dipole moments of charge transfer transitions are illustrated in Table VI which compares the configuration-interaction and improved virtual-orbital (or single-configuration) values for four transitions. Errors approaching an order of magnitude in the charge-transfer probabilities could result if configuration interaction were ignored.

IV. RATE COEFFICIENTS FOR RADIATIVE CHARGE TRANSFER

The rate coefficient for radiative charge transfer may be expressed as an integral of the transition probability over the collision path, averaged over the initial velocities and the impact parameters.[5] If we assume that the motion of the nuclei is classical and average over a Maxwellian velocity distribution, we obtain for the rate coefficient

$$k = 8\pi^{1/2} g \left(\frac{1}{kT}\right)^{3/2} \int_0^\infty dE \int_0^\infty dp \int_{R_0}^\infty dR \, \frac{pE^{1/2} A(R) \exp(-E/kT)}{[1 - p^2/R^2 - V(R)/E]^{1/2}} ,$$

where E is the kinetic energy at infinity, $V(R)$ is the entrance channel potential curve, $A(R)$ is the Einstein spontaneous emission transition probability, g is the statistical weight of the entrance channel, and R_0 is the classical distance of closest approach.

We fitted cubic spline functions through calculated values of the dipole moments and potential curves for interpolation, and, outside $R = 10a_0$, we adopted the appropriate long-range forms. Each of the potential curves was shifted to be consistent with the correct asymptotic limit. The transition

TABLE VIII. Total rate coefficients k for charge transfer in units of 10^{-14} cm^3 sec^{-1}.

T (K) \ Reaction	$C^{++}+H \rightarrow C^{+}+H^{+}+h\nu$	$C^{+++}+H \rightarrow C^{++}+H^{+}+h\nu$	$N^{++}+H \rightarrow N^{+}+H^{+}+h\nu$
10	1.59	6.48	2.40
30	1.55	6.32	2.38
100	1.50	6.12	2.40
300	1.39	5.94	2.28
1 000	1.28	5.62	2.10
3 000	1.35	5.32	2.04
10 000	1.71	5.50	2.14
30 000	2.12	6.40	2.50
100 000	2.44	8.22	3.16

probabilities were obtained using the expression

$$A_{nn'}(R) = \tfrac{4}{3}\alpha^3\omega^3_{nn'}(R)\,|D_{nn'}(R)|^2 \text{ a.u.},$$

where α is the fine-structure constant, and

$$\omega_{nn'}(R) = E_n(R) - E_{n'}(R).$$

The integrations were evaluated numerically for temperatures ranging from 10 to 100 000 K.

In calculating the rate coefficients we assumed that the nuclei move diabatically through the avoided crossings of the $3\,^3\Pi$ curve of $N^{++}-H$ and the $5\,^1\Sigma^+$ curve of $C^{+++}-H$. The assumption is surely valid for $N^{++}-H$ where the interaction is very small, but it is less certain for $C^{+++}-H$. However, for $C^{+++}-H$, radiative charge transfer is dominated by approach along the $2^3\Sigma^+$ potential. The results are presented in Tables VII A, VII B, and VII C.

In each system one transition dominates the reaction. For CH^{++} it is $2^2\Sigma^+ \rightarrow 1^2\Sigma^+$, for CH^{+++} it is $2^3\Sigma^+ \rightarrow 1^3\Sigma^+$, and for NH^{++} it is the $3^3\Pi \rightarrow 1^3\Pi$ transition. All are parallel transitions with $\Delta\Lambda = 0$. For an incoming state of a particular symmetry, the largest rate coefficient usually occurs for a transition to the lowest state of the same symmetry. The frequency factor enhances the probability of transition to the lowest state, and statistical weighting enhances triplets over singlets.

The total rate coefficients for reactions (3), (4), and (5), obtained by summing the values for individual transitions, are listed in Table VIII.

The rate coefficients are insensitive to temperature, varying by only a factor of 2 between 10 and 100 000 K, and relatively independent of the systems involved. At $T = 100$ K the total rates are 1.5×10^{-14} cm^3 sec^{-1} for C^{++}, 2.4×10^{-14} cm^3 sec^{-1} for N^{++}, and 6.1×10^{-15} cm^3 sec^{-1} for C^{+++}. At $T = 10^4$ K, the rates are, respectively, 1.7×10^{-14}, 2.1×10^{-14}, and 5.5×10^{-14} cm^{3}sec^{-1}.

The radiative process provides a lower limit to the total charge transfer rate and the rate coefficients are large enough that even in the absence of

TABLE IX. Final carbon $[3s/2p]$ basis set.

$1s$ exponents	Contraction coefficients
4232.61	0.001 221
634.882	0.009 348
146.097	0.045 490
42.497 4	0.154 796
14.189 2	0.359 244
1.966 55	0.144 818
5.147 73	0.438 998
5.147 73	−0.141 386
0.496 24	1.052 051
0.153 31	1.0
$2p$ exponents	
18.155 7	0.018 974
3.986 40	0.119 334
1.142 93	0.408 796
0.359 45	0.615 838
0.114 60	1.0

TABLE X. Final nitrogen $[3s/2p]$ basis set.

$1s$ exponents	Contraction coefficients
5909.44	0.001 190
887.451	0.009 104
204.749	0.044 159
59.837 6	0.150 580
19.998 1	0.357 048
2.685 98	0.143 936
7.192 74	0.447 445
7.192 74	−0.139 863
0.700 04	1.051 953
0.213 29	1.0
$2p$ exponents	
26.786 0	0.018 992
5.956 35	0.122 192
1.707 40	0.422 459
0.531 36	0.602 150
0.165 37	1.0

TABLE XI. Hydrogen [2s/2p] basis set.

1s exponents	Contraction coefficients
13.361 5	0.019 06
2.013 30	0.134 24
0.453 757	0.474 49
0.123 317	1.0
2p exponents	
0.557 104	0.325 65
0.129 568	0.785 41
0.095 40	1.0

crossings favorable to the nonradiative process, charge transfer plays a significant role in determining the ionization structure of fusion plasmas[6] and of gas clouds surrounding astrophysical x-ray sources.[7]

ACKNOWLEDGMENTS

This work was supported in part by the Energy Research and Development Administration under Contract No. EY-76-S-02-2887. The authors are grateful to Dr. T. H. Dunning for the use of his configuration interaction properties program for calculation of the transition moments.

APPENDIX: BASIS SET

The primitive (9s/5p) basis set used for describing orbitals centered on the C or N nucleus is that of Huzinaga.[2] The orbital exponents for the Gaussian-type radial functions are listed in Tables IX and X. The contraction coefficients listed were computed from atomic self-consistent-field calculations. Calculations were done for C^+, C^{++}, N^+, and N^{++}. For nitrogen, the resulting sets of contraction coefficients were averaged to create an unbiased set. For carbon, the C^+ and the C^{++} coefficients of the 6s primitive in the first two contracted s orbitals were averaged to produce an unbiased set. The normalized [3s/2p] basis sets used throughout the calculation are listed in Tables IX and X.

The hydrogen 1s orbital was described by four s-type Gaussian orbitals contracted into two s-type contracted Gaussian orbitals. The exponents and contraction coefficients are those of Huzinaga. To obtain the correct charge-dipole polarization effects we added a 2p orbital (represented by two contracted Gaussians) with an effective Slater exponent of 1.0 and a 3p orbital[8] (represented by a single Gaussian) with an effective Slater exponent of 1.0 to the hydrogen-centered basis set. Table XI lists the hydrogen (2s/2p) basis set.

In situations where the electrons are less tightly bound, d-type orbitals centered on the heavy nucleus need to be included in order to describe polarization effects correctly. We found that the effects of the d orbitals were small, providing at most an energy improvement of 0.04 eV even at internuclear distances as small as 2.0 a_0.

[1]D. R. Bates and B. L. Moiseiwitsch, Proc. Phys. Soc. A 67, 805 (1954); A. Dalgarno, *ibid.* 67, 1010 (1954); R. McCarroll and P. Valiron, Astron. Astrophys. 44, 465 (1975); R. J. Blint, W. D. Watson, and R. B. Christensen, Astrophys. J. 205, 634 (1976); R. McCarroll and P. Valiron, Astron. Astrophys. 53, 83 (1976).

[2]S. Huzinaga, J. Chem. Phys. 42, 1293 (1965).

[3]T. H. Dunning, J.Chem. Phys. 53, 2823 (1970).

[4]W. J. Hunt and W. A. Goddard, Chem. Phys. Lett. 3, 414 (1969).

[5]D. R. Bates, Mon. Not. R. Astron. Soc. 111, 303 (1951).

[6]Cf. H. P. Furth, Nucl. Fusion 15, 487 (1975).

[7]R. McCray, C. Wright, and S. Hatchett, Astrophys. J. Lett. 211, L29 (1977).

[8]Cf. A. Dalgarno, Adv. Phys. 11, 281 (1962).